AIAA JOURNAL
Vol. 41, No. 2, February 2003

Thermally Induced Vibrations of Spinning Thin-Walled Composite Beam

Kyung-Eun Ko* and Ji-Hwan Kim†
Seoul National University, Seoul 151-742, Republic of Korea

Coupled thermal–structural analysis, which includes the interaction between structural deformations and incident heating, is performed for spinning thin-walled composite beam appendages. The beam model is assumed to have transverse shear deformation and rotary inertia, as well as primary and secondary warping effects. Additionally, the thermal flutter problem is studied by the stability analysis of the beam. For the thermal analysis, the two-dimensional heat transfer in the axial and circumferential directions of a thin-walled beam is considered; the changes of the heating surface should be involved due to the spinning motion of the beam. The thermal and the structural analyses are based on the principle of conservation of energy and Hamiltons principle, respectively. Numerical results are compared with those of the uncoupled analysis. A steady-state thermal response can be determined by the uncoupled analysis, whereas thermal flutter may be studied by the coupled thermal–structural analysis. Also, the coupled analysis provides data on the stability characteristics, as well as dynamic responses. Furthermore, the spinning speed plays an important role in the stability of the spinning beam under solar heat flux. When the spinning speed is equal to the bending frequency of the beam, then the structure is unconditionally unstable.

Nomenclature

A	=	beam cross-sectional area
C	=	contour of the cross section of the thin-walled beam
c	=	specific heat
H	=	thickness of thin-walled beam
k	=	thermal conductivity
L	=	length of thin-walled beam
N	=	number of layers of the thin-walled beam
q	=	normal direction of beam surface
R	=	radius of thin-walled beam
S_0	=	solar heat flux
u_α	=	displacements of axis, where $\alpha = 1, \ldots, 3$
v_0, w_0	=	translational displacements along the y and z axis
α	=	absorptivity
α_T	=	coefficient of thermal expansion
β	=	solar incident angle
ε	=	emissivity
ζ	=	damping coefficient
Θ	=	temperature
Θ_{med}	=	medium temperature
Θ_0	=	initial temperature
θ	=	fiber angle of layer
ρ	=	density
σ	=	Stefan–Boltzmann constant
τ	=	thermal response time
φ	=	angular coordinate
Ω	=	spinning speed
$'$	=	$\mathrm{d}(\,)/\mathrm{d}x$

Received 23 February 2002; presented as Paper 2002-1623 at the 43rd Structures, Structural Dynamics, and Materials Conference, Denver, CO, 22–25 April 2002; revision received 12 July 2002; accepted for publication 17 July 2002.

*Graduate Research Assistant, School of Mechanical and Aerospace Engineering; currently Research Engineer, Hyundai Heavy Industries Co., Ltd., 1, Cheonha-Dong, Dong-Ku, Ulsan 682-792, Republic of Korea.

†Associate Professor, School of Mechanical and Aerospace Engineering, San 56-1, Shinrim-Dong, Kwanak-Ku. Member AIAA.

Introduction

WHEN a spacecraft makes an orbital eclipse transition as it exits from or enters into the Earths shadow, vibrations may develop because of rapid changes in the thermal loading of appendages. By the unexpected displacements or accelerations, the spacecraft appendages may degrade system operations. Practically, interaction of structural deformations and incident heating may induce unstable vibrations of the appendages, which may result in spacecraft failure. Consequently, stability problems such as thermal flutter have been investigated by the use of thermally induced bending or torsional vibrations for the booms and solar arrays. Tsuchiya[1] studied the thermally induced vibrations of an appendage attached to a spacecraft. He paid special attention to the behavior of structures near the resonance condition and found that the resonance occurred as the natural frequency of the appendage is approximately equal to twice or half of the nutational frequency. Johnston and Thornton[2] analyzed the effects of thermally induced structural disturbances of an appendage on the dynamics of a simple spacecraft. Numerical results showed that the system dynamic response consisted of a slowly developed pointing error and superimposed oscillations, whose magnitude was related to the ratio of the thermal and structural response times of the appendage. Chung and Thornton[3] investigated the failure mechanism of a solar array boom. The solar array was deployed with a membrane tension that induced the boom compressive force, which was almost equal to the boom critical force for torsional buckling of the solar array. They also studied the unexpected vibration disturbances during eclipse transition.

Two types of analyses have been developed to study thermally induced vibrations: uncoupled or the coupled thermal–structural analyses. Previously, most researchers used uncoupled thermal–structural analysis, which assumes that heating and temperature gradients are not affected by the structural motion. Boley[4] was the first to consider the inertia effects in calculating the thermal–structural response of a beam under rapid heating, and Boley[5] derived a simple general formula for the maximum ratio of the dynamic to the static deflection of heated beams and plates. Additionally, these papers showed that thermally induced vibrations may occur when the structural and thermal response times are of the same order of magnitude. Tamma et al.[6] used a generalized transform method based on the finite element method in the dynamic analysis, and they studied the transient responses of an Euler–Bernoulli beam under rapid heating. Manolis and Beskos[7] investigated the dynamic responses of beam structures under suddenly applied thermal load. The Laplace

transform method was used with the dynamic stiffness influence coefficients. Lutz et al.[8] proposed different finite element models for thermal and structural analysis of frame-type structures, and they determined temperature fields on the selected cross sections of beam members. Then, the forces and moments generated by the temperature distribution were calculated, and the global response of the structure was obtained in the three-dimensional frame.

Generally, uncoupled thermal–structural analysis cannot describe the unstable motion of structure, whereas coupled thermal–structural analysis, which includes the effects of structural deformations on heating and temperature gradients, can follow the unstable motion that may be induced by the sudden thermal loading. In this regard, the stability characteristics of the coupled analysis have been also studied. Thornton and Kim[9] adopted an analytical approach to obtain the thermal–structural response of a rolled-up solar array due to the sudden increase of the external heating, and the results were compared with the uncoupled analysis responses. Additionally, the stability criteria established the conditions for thermal flutter. Thornton et al.[10] developed an approach to analyze the thermally induced vibrations of a split-blanket solar array due to self-shadowing of the central truss. The results showed that parallel-member shadowing can develop thermally induced vibrations, whereas cross-member shadowing can not induce the same phenomena.

Spinning motion plays an important role in space structures. Leung and Fung[11] used the finite element method to analyze spinning structures. Because the beam member is oriented arbitrarily relative to a rotating frame, general spinning structures can be considered. Gulick and Thornton[12] studied the thermally induced vibrations of the axial boom for a spin-stabilized spacecraft. The uncoupled analysis may provide the steady-state thermal response, whereas the coupled analysis can be used to investigate the unstable behavior of spinning structures. Farmer et al.[13] studied the effects of the geosynchronous thermal environment on the surface accuracy of a tetrahedral-truss support structure for a high-frequency microwave antenna. They emphasized that the thermal environment and the slow rotation of the spacecraft relative to the sun result in long exposure to both heat and cold, thus setting severe temperature extremes.

Large space structures are typically made up of three-dimensional truss-type structures, and they are almost always composed of the composite materials with high-strength and low-density properties. Givoli and Rand[14] analyzed the large truss-type space structures undergoing periodic motion by using Fourier decomposition and the finite element method. The numerical results of the thermal and elastic analysis described the transition between the quasi-steady state and the dynamic state. Thornton and Paul[15] reviewed the modeling, analysis and thermal–structural responses of large spacecraft. Givoli and Rand[16] devised a numerical scheme for the open-loop optimal control of thermoelastic deformation for cylindrical-shaped truss structures. Four different cost functionals were considered; they involved the elastic deformation of structure and included penalties on the control magnitudes.

In this study, the coupled thermal–structural problem of spinning composite thin-walled beam appendages is analyzed, and the stability characteristics are also studied. The derived external force vector of the solar heat flux includes the thermal–structural coupling terms. A structural model is generated based on the thin-walled beam theory with the transverse shear deformation and the rotary inertia, as well as primary and secondary warping effects. In the thermal analysis, the two-dimensional heat transfer in the axial and circumferential directions of the beam is considered. Furthermore, the spinning motion of the beam results in the change of the heating surface, which is to be considered. The thermal and the structural analysis are based on the conservation of energy and Hamilton's principle, respectively. Numerical results are based on the finite element method. Additionally, the Newton–Raphson iteration method and the Newmark direct integration method are used to solve the coupled nonlinear equations for each time step. Then the results of the coupled thermal–structural analysis are compared with those of the uncoupled analysis. Dynamic analysis of the appendages is performed for various solar incident angles and the ply angles of the composite materials. In addition, the stability characteristics of the spinning thin-walled composite beam are studied in detail.

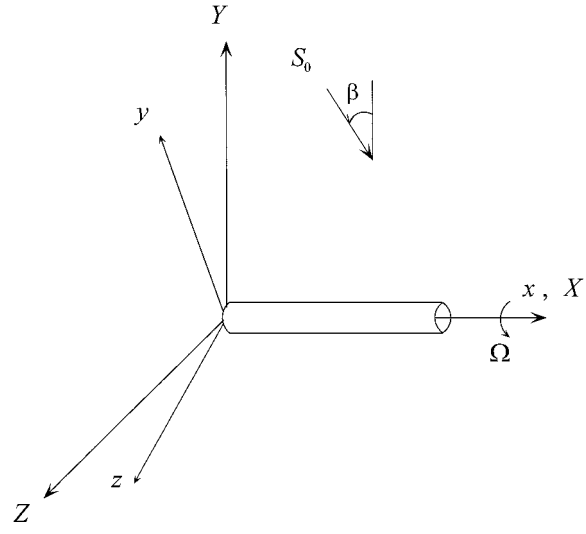

Fig. 1 Spinning thin-walled beam with the solar heat flux S_0.

Formulation

Modeling and Basic Assumptions

Figure 1 shows the spinning composite thin-walled beam with the solar heat flux S_0. XYZ is the inertial reference frame, and xyz is the body-fixed reference frame rotating about the X axis. In this study, following assumptions are considered:

1) The absorbed heat flux depends on the deformations of the beam.

2) The incident solar heat flux S_0 is constant, parallel to the XY plane.

3) The thermal energy is emitted from the external surface of the beam similar to the diffuse radiation, and the internal radiation within the beam is neglected.

4) The temperature is constant across the thickness of the beam wall.

5) The cross sections of the beam remain in their own planes.

6) The thin-walled beam theory is applied to the analysis of the structural model with considerations to the transverse shear deformation and the rotary inertia, as well as the primary and secondary warping effects.

Coupled Thermal–Structural Analysis

Thermal Analysis

Figure 2a shows the thin-walled beam model under the solar heat flux S_0, and the normal direction with respect to the deformed state of the beam is q. The beam slope, $\mathrm{d}V/\mathrm{d}x$, is defined in the inertial reference frame, and V is the translational displacement along the Y axis. Figure 2b shows a cross section of the heating surface of the spinning beam.

Heat transfer is assumed to occur in the axial, x, and circumferential, φ, directions simultaneously, then

$$k\left(\frac{\partial^2\Theta}{\partial x^2}+\frac{1}{R^2}\frac{\partial^2\Theta}{\partial\varphi^2}\right)+\frac{\sigma\varepsilon}{h}\left(\Theta_{\mathrm{med}}^4-\Theta^4\right)+\frac{\alpha}{h}S_0\delta\cos(\varphi+\Omega t)\cos\left(\beta-\frac{\partial V}{\partial x}\right)=\rho c\frac{\partial\Theta}{\partial t} \tag{1}$$

where $\delta = 1$ or 0 indicates that the side of the beam is either heated or not heated. The second term on the left-hand side describes the diffusion radiation from external surface of the beam, and the third term defines the solar heat flux. The term $\cos(\beta - \partial V/\partial x)$, which expresses the effect of structural deformation on the incident heat flux, is the thermal–structural coupling term that is ignored in the uncoupled thermal–structural analysis.

The initial condition is expressed as

$$\Theta(\varphi, x, 0) = \Theta_0 \tag{2}$$

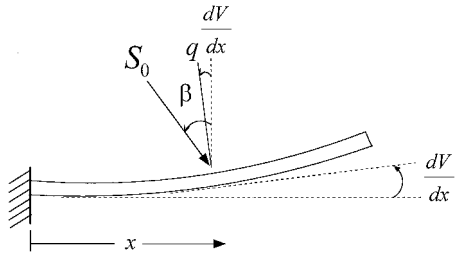

Fig. 2a Heat flux for the coupled thermal–structural analysis.

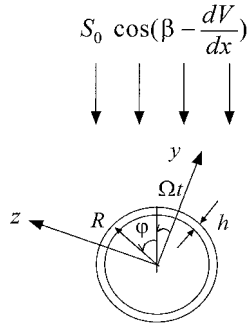

Fig. 2b Heat surface beam cross section.

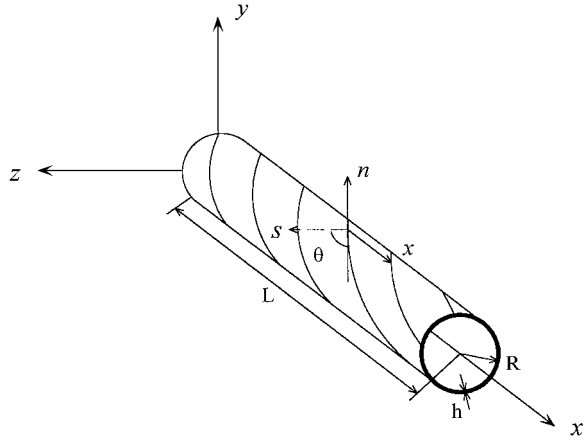

Fig. 3 Composite thin-walled beam with circular cross section.

Structural Analysis

Figure 3 shows the composite thin-walled beam, and *sxn* is the local coordinate system defining the contour, length, and thickness directions, respectively.

To get the thin-walled beam model, the displacement fields is assumed to be as in Ref. 17:

$$u_1(s,x,n,t) = u_0(x,t) - \theta_y(x,t)\left[z(s) - n\frac{\mathrm{d}y}{\mathrm{d}s}\right] - \theta_z(x,t)\left[y(s) + n\frac{\mathrm{d}z}{\mathrm{d}s}\right] - \phi'(x,t)[F_w(s) + na(s)]$$

$$u_2(s,x,t) = v_0(x,t) - z(s)\phi(x,t)$$

$$u_3(s,x,t) = w_0(x,t) + y(s)\phi(x,t) \tag{3}$$

where $\theta_y(x,t)$, $\theta_z(x,t)$, and $\phi(x,t)$ are the rotations about the y and z axes and twist about the x axis, respectively. In addition, $F_w(s)$ and $na(s)$ are the primary and secondary warping functions.

Then the strain–displacement relations are

$$\varepsilon^0_{xx}(s,x,t) = u_0'(x,t) - \theta_y'(x,t)z(s) - \theta_z'(x,t)y(s) - \phi''(x,t)F_w(s)$$

$$\varepsilon^n_{xx}(s,x,t) = \theta_y'(x,t)\frac{\mathrm{d}y}{\mathrm{d}s} - \theta_z'(x,t)\frac{\mathrm{d}z}{\mathrm{d}s} - \phi''(x,t)a(s)$$

$$\gamma^0_{sx}(s,x,t) = [v_0'(x,t) - \theta_z(x,t)]\frac{\mathrm{d}y}{\mathrm{d}s} + [w_0'(x,t) - \theta_y(x,t)]\frac{\mathrm{d}z}{\mathrm{d}s}$$

$$\gamma^t_{sx}(s,x,t) = 2\frac{A_c}{\beta_c}\phi'(x,t)$$

$$\gamma_{xn}(s,x,t) = [v_0'(x,t) - \theta_z(x,t)]\frac{\mathrm{d}z}{\mathrm{d}s} - [w_0'(x,t) - \theta_y(x,t)]\frac{\mathrm{d}y}{\mathrm{d}s} \tag{4}$$

where A_c and β_c are the cross-sectional area of the boom bounded by the midline contour and the circumferential contour length, respectively.

The three-dimensional constitutive equations of generally orthotropic materials can be integrated along the thickness direction. Then, the resultant forces N_{xx} and N_{sx}, transverse shear resultant force N_{xn}, and resultant moments L_{xx} and L_{sx}, including the thermal effects, can be expressed as

$$\begin{bmatrix} N_{xx} \\ N_{sx} \\ L_{xx} \\ L_{sx} \\ N_{xn} \end{bmatrix} = \begin{bmatrix} K_{11} & K_{12} & K_{13} & K_{14} & 0 \\ K_{21} & K_{22} & K_{23} & K_{24} & 0 \\ K_{41} & K_{42} & K_{43} & K_{44} & 0 \\ K_{51} & K_{52} & K_{53} & K_{54} & 0 \\ 0 & 0 & 0 & 0 & A_{44} \end{bmatrix} \begin{bmatrix} \varepsilon^0_{xx} \\ \gamma^0_{sx} \\ \gamma^t_{sx} \\ \varepsilon^n_{xx} \\ \gamma^0_{xn} \end{bmatrix} - \begin{bmatrix} N_1^T \\ N_2^T \\ N_4^T \\ N_5^T \\ 0 \end{bmatrix} \tag{5}$$

where K_{ij}, $i \neq 3$ and $j \neq 5$, A_{44}, and N_i^T, $i \neq 3$, are the modified stiffnesses, extensional stiffness, and thermal resultant forces and are expressed as in Ref. 17.

The strain energy of the deformation in the thin-walled composite beam can be written as

$$U = \frac{1}{2}\int_0^L \int_C \sum_{k=1}^{N} \int_{h^{(k)}} [\sigma_{xx}\varepsilon_{xx} + \sigma_{sx}\gamma_{sx} + \sigma_{xn}\gamma_{xn}]^{(k)}\,\mathrm{d}n\,\mathrm{d}s\,\mathrm{d}x$$

$$= \frac{1}{2}\int_0^L \int_C \left[N_{xx}\varepsilon^0_{xx} + L_{xx}\varepsilon^n_{xx} + N_{sx}\gamma^0_{sx} + \left(2\frac{A_c}{\beta_c}\right)N_{sx}\phi' + N_{xn}\gamma_{xn}\right]\mathrm{d}s\,\mathrm{d}x \tag{6}$$

The position vector $\{\boldsymbol{r}\}$ and the velocity vector $\{\boldsymbol{v}\}$ of a point on the deformed thin-walled beam can be expressed as in Ref. 11:

$$\{\boldsymbol{r}\} = \{\boldsymbol{r}_0\} + \{\boldsymbol{u}\} \tag{7}$$

$$\{\boldsymbol{v}\} = \{\dot{\boldsymbol{r}}\} + [\boldsymbol{\Omega}]\{\boldsymbol{r}\} = \{\dot{\boldsymbol{u}}\} + [\boldsymbol{\Omega}](\{\boldsymbol{r}_0\} + \{\boldsymbol{u}\}) \tag{8}$$

where $\{\boldsymbol{r}_0\}$ is the position vector of the undeformed beam and the spinning matrix $[\Omega]$ is defined as

$$[\Omega] = \begin{bmatrix} 0 & 0 & 0 \\ 0 & 0 & -\Omega \\ 0 & \Omega & 0 \end{bmatrix} \tag{9}$$

Then the kinetic energy with the spinning motion is

$$T = \frac{1}{2}\int_0^L \int_C \int_{-h/2}^{h/2} \rho\{\boldsymbol{v}\}^T\{\boldsymbol{v}\}\,\mathrm{d}n\,\mathrm{d}s\,\mathrm{d}x \tag{10}$$

When formulas (6) and (10) are used for the potential energy and the kinetic energy, the equations of motion can be derived by Hamilton's principle as in Ref. 17:

$$\delta\int (T - U)\,\mathrm{d}t = 0 \tag{11}$$

Finite Element Method

Governing Equation

When the finite element method is applied, the matrix form of the coupled thermal–structural equations of motion can be written as follows:

For the thermal analysis, the equations of motion (1) become

$$[\boldsymbol{C}_\Theta]\{\dot{\boldsymbol{\Theta}}\} + [\boldsymbol{K}_\Theta]\{\boldsymbol{\Theta}\} = \{\boldsymbol{F}_\Theta(\boldsymbol{U},\boldsymbol{\Theta})\} \tag{12}$$

where $[\boldsymbol{C}_\Theta]$, $[\boldsymbol{K}_\Theta]$, $\{\boldsymbol{F}_\Theta\}$, and $\{\boldsymbol{\Theta}\}$ are the heat capacity matrix, conduction matrix, conduction vector due to the radiation, and temperature vector, respectively.

For the structural analysis, the equations of motion (11) become

$$[\boldsymbol{M}]\{\ddot{\boldsymbol{U}}\} + [\boldsymbol{C}_G]\{\dot{\boldsymbol{U}}\} + ([\boldsymbol{K}_E] + [\boldsymbol{K}_\Omega])\{\boldsymbol{U}\} = \{\boldsymbol{F}(\boldsymbol{\Theta})\} \tag{13}$$

where $[\boldsymbol{M}]$, $[\boldsymbol{C}_G]$, $\{\boldsymbol{F}\}$, and $\{\boldsymbol{U}\}$ are the mass matrix, gyroscopic matrix, external force vector due to thermal moment, and displacement vector, respectively. In addition, $[\boldsymbol{K}_E]$ and $[\boldsymbol{K}_\Omega]$ are the elastic stiffness matrix and the stiffness matrix of the spinning motion of the beam, respectively.

Two sets of Eqs. (12) and (13) are coupled by the term $\{\boldsymbol{F}(\boldsymbol{\Theta})\}$ and $\{\boldsymbol{F}_\Theta(\boldsymbol{U}, \boldsymbol{\Theta})\}$; thus, the nonlinear equations must be solved simultaneously. The Newton–Raphson iteration and Newmark direct integration methods (see Ref. 18) are used to solve the the coupled nonlinear equations.

Stability Analysis

The modal analysis of the stability problem is assumed be based on the lowest mode because the structural response mainly depends on the first mode vibration.

For the beam without spinning motion, the lowest modal equation with the modal damping can be written as

$$\ddot{X}_1 + 2\zeta\omega_1\dot{X}_1 + \omega_1^2 X_1 = \{\Phi\}_1^T\{\boldsymbol{F}\} \tag{14}$$

where ω_1 and $\{\Phi\}_1$ are the natural frequency and modal vector of the first mode for the free vibration. Additionally, $\{\boldsymbol{F}\}$ can be obtained by using the analytical solution of the circumferential heat transfer.[9] The effects of the axial heat transfer can be neglected when compared with the circumferential heat transfer. Laplace transform and the Routh–Hurwitz test are used in Eq. (14) to study the stability characteristics.

Then, the stability region is

$$\eta < (2\zeta\kappa^2 + 4\zeta^2\kappa + 2\zeta)/\kappa \tag{15}$$

where $\kappa = 1/\omega_1\tau$ and $\eta = \alpha_T\Theta^*(\boldsymbol{B}/R)\sin\beta$. Additionally, Θ^* is the steady-state perturbation temperature, and

$$\boldsymbol{B} = \{\Phi\}_1^T E I \int_0^L \left[\boldsymbol{B}_{\theta_z}\right]^T [\boldsymbol{B}_v]\,\mathrm{d}x \frac{\{\Phi\}_1}{\omega_1^2}$$

The stability of the spinning beam may be analyzed by the lowest two modal equations, and they become

$$\begin{aligned}
&\ddot{X}_1 + 2\zeta\omega_1\dot{X}_1 - 2\Omega\dot{X}_2 + \left(\omega_1^2 - \Omega^2\right)X_1 = \{\Phi\}_1^T\{\boldsymbol{F}\} \\
&\ddot{X}_2 + 2\zeta\omega_2\dot{X}_2 + 2\Omega\dot{X}_1 + \left(\omega_2^2 - \Omega^2\right)X_2 = \{\Phi\}_2^T\{\boldsymbol{F}\}
\end{aligned} \tag{16}$$

Now $\{\boldsymbol{F}\}$ is obtained by using the analytical solution for the circumferential heat transfer.[12] As with the beam without spinning, the effects of the axial heat transfer can be neglected.

Floquet theory may be applied to analyze the stability of the spinning beam; the theory establishes the stability of linear ordinary differential equations with periodic coefficients.

Numerical Results and Discussion

In this work, we mainly consider the results obtained by the coupled thermal–structural analysis of the spinning composite thin-walled beam.

Code Verifications

Figure 4 shows the natural frequencies of the spinning beam without thermal loading. The first two dimensionless natural frequencies at various spinning rates are compared with previous work.[11] The numerical results agree well with the lateral bending and the transverse bending mode.

Table 1 shows the natural frequencies of the composite box beam without thermal loading. The first two natural frequencies of the lateral and the transverse bending mode are compared with previous work,[17] and the results agree well regardless of layer angles.

Figures 5a–5c show the numerical results of the nonspinning beam and are compared with the data[9] that deal with the dynamic behavior of the Hubble Space Telescope (HST) solar array. Based on the uncoupled analysis, the results are fairly good agreement.

Figure 6 shows the unstable beam response from the coupled analysis of the HST solar array for the solar incident angle $\beta = 80$ deg and damping coefficient $\zeta = 10^{-4}$. The results of the previous work,[9] and the present data agree fairly well. A slight discrepancy, about

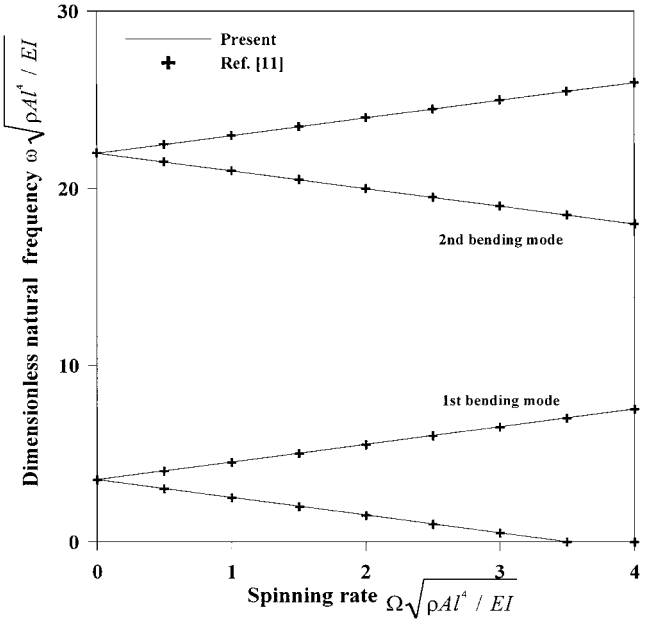

Fig. 4 Dimensionless natural frequency of the spinning beam.

Table 1 Box beam case: first two eigenfrequencies (rad/s) for the lateral bending mode and transverse bending mode

	Lateral bending mode				Transverse bending mode			
	Fundamental		Second		Fundamental		Second	
Ply angle, deg	Ref. 17	Present	Ref. 17	Present	Ref. 17	Present	Ref. 17	Present
0	871	870.3 (−0.08)[a]	——	4330.9	249	249.3 (+0.12)	1558	1556 (−0.13)
15	881	880.9 (−0.01)	4383	4380.1 (−0.07)	253	252.2 (−0.31)	1577	1573.7 (−0.21)
30	949	948.1 (−0.09)	4657	4653.6 (−0.07)	269	268.2 (−0.30)	1676	1673.8 (−0.13)
45	1236	1236.3 (+0.02)	5490	5480.1 (−0.18)	318	317.4 (−0.19)	1985	1981.1 (−0.20)
60	2182	2181.6 (−0.02)	7554	7529.5 (−0.32)	443	441.7 (−0.29)	2786	2776.1 (−0.35)
75	3916	3912.3 (−0.09)	12333	12293 (−0.32)	765	762.1 (−0.38)	4934	4919.1 (−0.30)
90	4583	4582.2 (−0.02)	——	18062	1502	1500.5 (−0.10)	8502	8509.2 (+0.08)

[a] Values in parentheses are percentage difference.

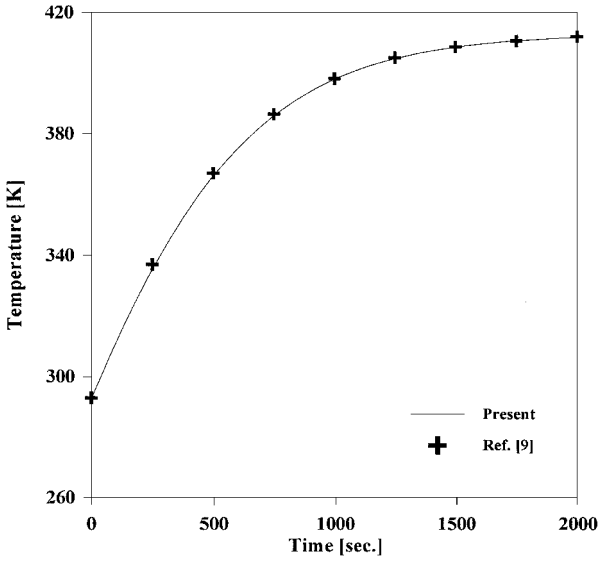

Fig. 5a Average temperature of the beam.

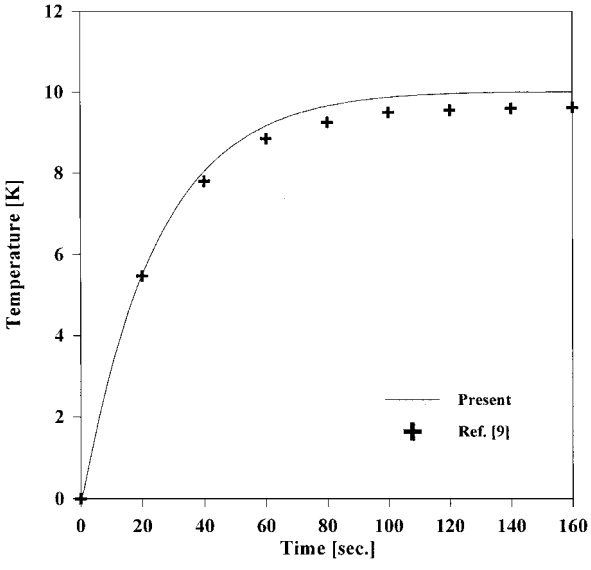

Fig. 5b Perturbation temperature of the beam.

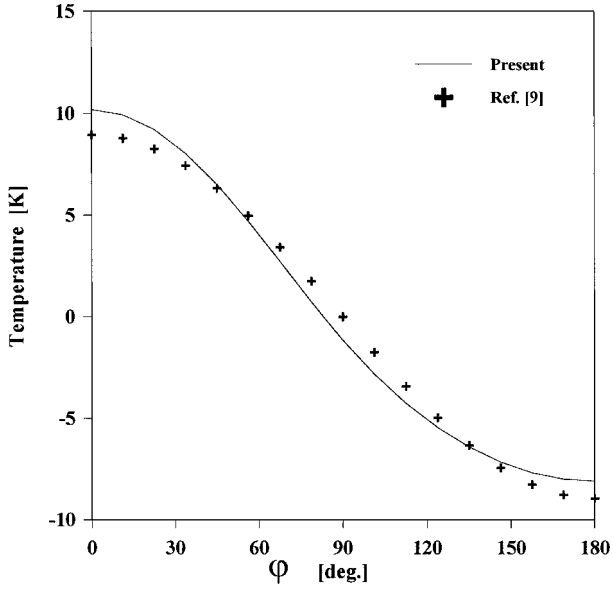

Fig. 5c Temperature distributions along the cross section of the beam at time equals 60 s.

Table 2 Data from Ref. 9

Parameter	Value
α	0.5
α_T, m/m · K	1.692$E-5$
S_0, W/m^2	1.350$E+3$
σ, W/m^2 · K^4	5.670$E-8$
ε	0.13
c, J/kg · K	5.020$E+2$
ρ, kg/m^3	7.010$E+3$
h, m	2.35$E-4$
k, W/m · K	1.661$E+1$
R, m	1.092$E-2$
E, N/m^2	1.930$E+11$
L, m	5.91
m_{tip}	1.734

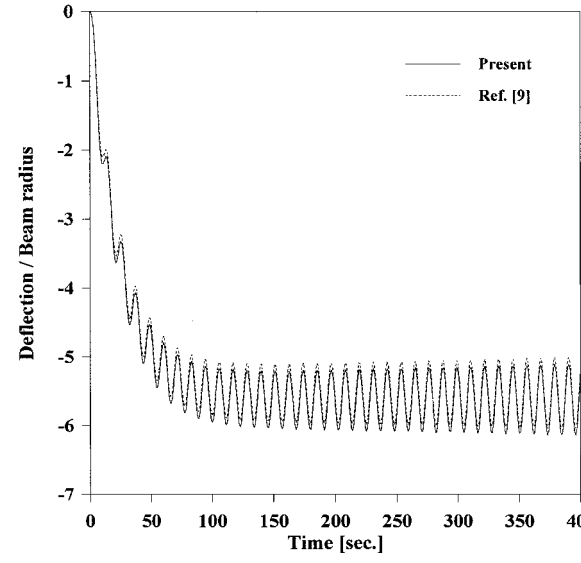

Fig. 6 Comparison of the coupled analysis for the unstable beam deflection.

2%, may be due to the difference between the analytical approach and finite element approach. It is also discussed in Ref. 9.

Dynamic Analysis

Figure 7 expresses the quasi-static and dynamic deflection responses of the tip of a nonspinning beam. The solar incident angle $\beta = 80$ deg and damping coefficient $\zeta = 0$ are used, and the tip mass $m_{\text{tip}} = 1.734$ kg is chosen as in Ref. 9. The dotted line and the solid line stand for the uncoupled thermal–structural analysis and coupled thermal–structural analysis results, respectively. The dotted line shows the constant dynamic deflection response after for about 120 s, whereas the solid line shows the increasing dynamic deflection response due to the interaction of the temperature gradients and the deflection of beam. As a result, coupled thermal–structural analysis must be performed to investigate the unstable motions that may be induced by the solar heat flux.

Figures 8 and 9 show the dynamic response of the beam obtained from the coupled thermal–structural analysis. Table 2 shows the solar array data for the HST,[9] and we choose to use these data.

Figure 8 shows the quasi-static and dynamic deflections of the beam tip for various solar incident angles. As the solar incident angle is increased, the deflection is decreased because of the reduction of the normal component of the heat flux. Figure 9 shows the quasi-static and dynamic deflections of the beam tip for two typical kinds of the ply angles of composite materials. As a composite material, we select the graphite–epoxy as follows:

$$E_1 = 294 \text{ GPa}, \qquad E_2 = E_3 = 6.4 \text{ GPa}, \qquad G_{12} = 4.9 \text{ GPa}$$

$$\nu_{12} = \nu_{23} = \nu_{13} = 0.23, \qquad \nu_{21} = \nu_{32} = \nu_{31} = 0.01$$

$$\alpha_{T1} = -0.1 \times 10^{-6} \text{ K}, \qquad \alpha_{T2} = \alpha_{T3} = 26 \times 10^{-6} \text{ K}$$

$$k = 41.5 \text{ W/m} \cdot \text{K}, \qquad c = 880 \text{ J/kg} \cdot \text{K}$$

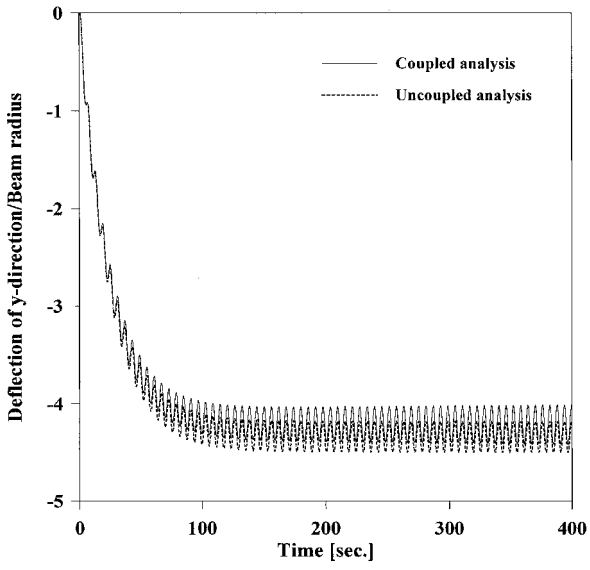

Fig. 7 Comparison between coupled and uncoupled thermal–structural analysis.

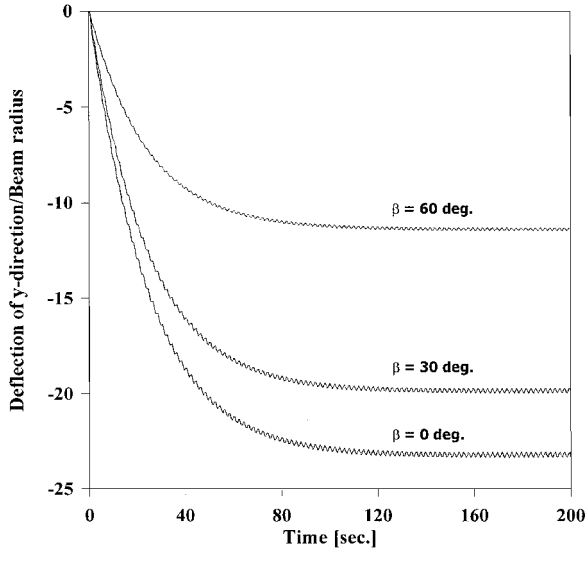

Fig. 8 Beam deflection with respect to the solar incident angle.

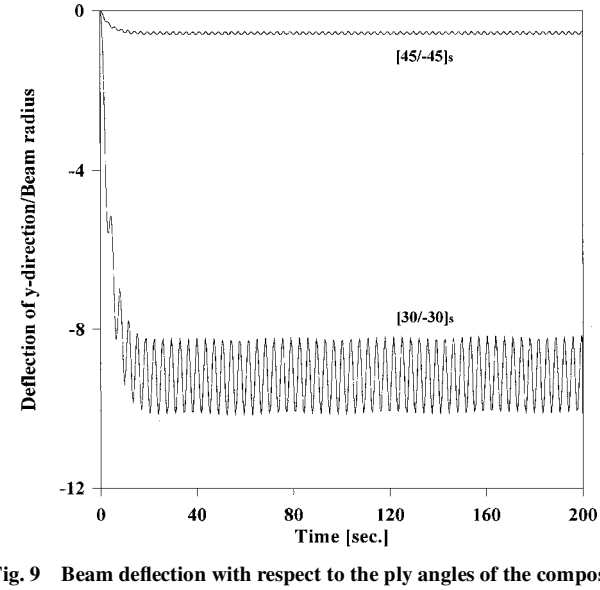

Fig. 9 Beam deflection with respect to the ply angles of the composite materials.

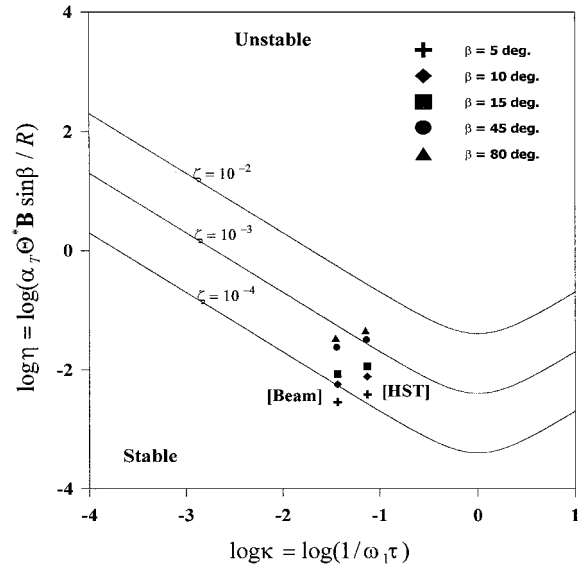

Fig. 10 Stability boundary of HST solar array and beam.

The solar incident angle $\beta = 0$ and the damping coefficients $\zeta = 0$ are chosen to use. The quasi-static and dynamic deflections of the $[45/-45]_s$ stacking sequence are less than for the $[30/-30]_s$ sequence. The appropriate stacking sequence of the composite materials can control the deflections of the structures.

Stability Criterion

Figure 10 shows the stability boundaries of the HST solar array[9] and of the isotropic[9] beam using Eq. (17). The horizontal axis κ is the ratio of the structural response time to thermal response time. The vertical axis η is the measure of the thermally induced response that accounted for the coefficient of thermal expansion, steady-state perturbation temperature, and solar incident angle. The stability boundaries are plotted with respect to the various damping coefficients $\zeta = 10^{-2}$, 10^{-3}, and 10^{-4}. The dimensionless parameters κ and η and the damping coefficient ζ play an important role in the stability criterion of structures. When the structural response time of the beam is equal to its thermal response time, as $\kappa = 1$, then the stable region is the least value as shown in Fig. 10. As a result, the structure is more stable as the value of η is decreased, and κ is far from 1 and ζ is increased.

Figure 11 shows the stability boundaries of the isotropic beam. As the length is increased, then the unstable region becomes wider due to the increase of the flexibility. Figures 12a and 12b indicate the stable and the unstable deflection response in Fig. 11, respectively.

Figure 13 describes the stability boundaries of the composite beam for the stacking sequence of $[45/-45]_s$. Similar to the isotropic beam, the unstable regions become wider as the length is increased. Figure 14 shows the stability boundaries of the composite beam with respect to the various stacking sequences of the materials, and the $[0/45/-45/90]_s$ sequence results in the larger stable region for the various damping coefficients than the other cases. For this region, the appropriate stacking sequence of the composite materials can increase the stable region of the structures.

Figures 15 and 16 show the stability boundaries of the spinning beam for the coupled thermal–structural analysis. Figure 15 shows the stability boundaries of the spinning isotropic beam with the results from Ref. 13. The horizontal axis μ is the ratio of the spinning speed and the bending frequency of the beam, and the vertical axis η is the measure of the thermally induced response. The stability boundaries of the spinning beam are plotted with respect to various damping coefficients $\zeta = 2 \times 10^{-3}$, 1×10^{-3}, and 5×10^{-4}. As μ is decreased, the stable region becomes wider. The spinning speed plays an important role in the stability characteristics of the spinning beam under the solar heat flux. In the case where the spinning speed equals the bending frequency of the beam, the beam structure is unconditionally unstable. The solar flux data in Fig. 15 express the state of the spinning beam with the heat flux. Figure 16 shows that

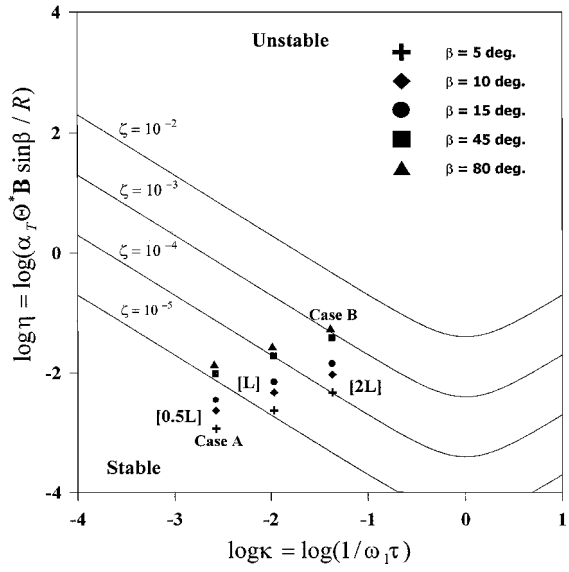

Fig. 11 Stability boundary with respect to the length of the isotropic beam.

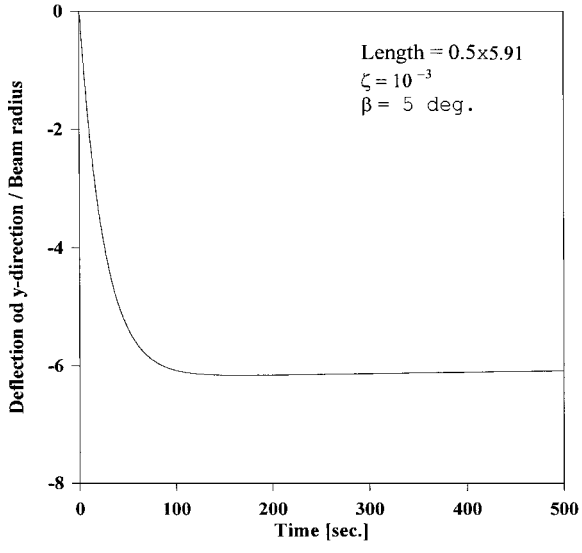

Fig. 12a Case A in Fig. 11.

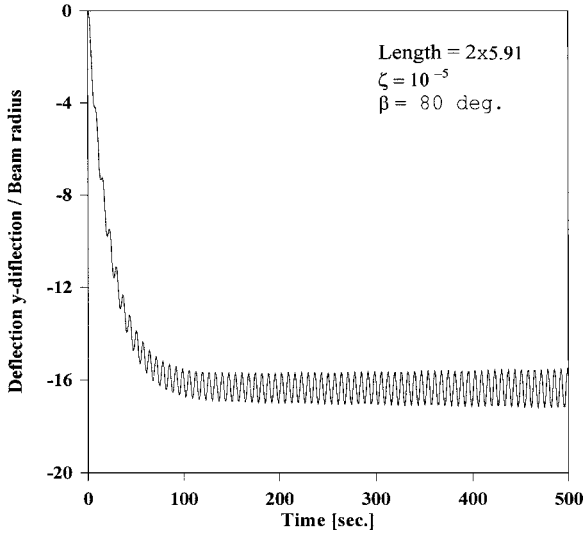

Fig. 12b Case B in Fig. 11.

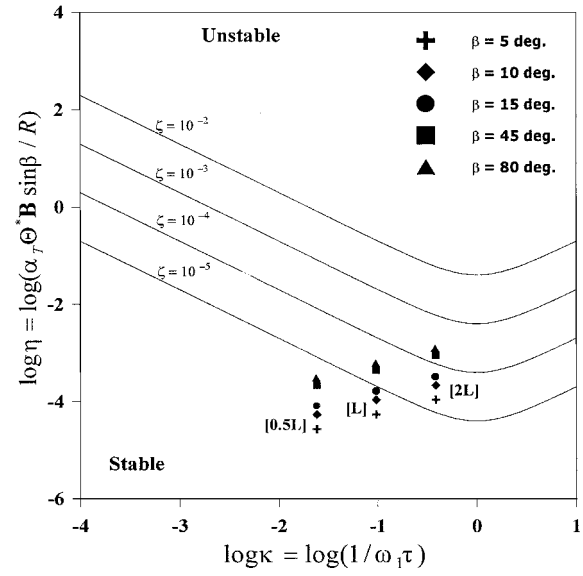

Fig. 13 Stability boundary with respect to the length of the composite beam.

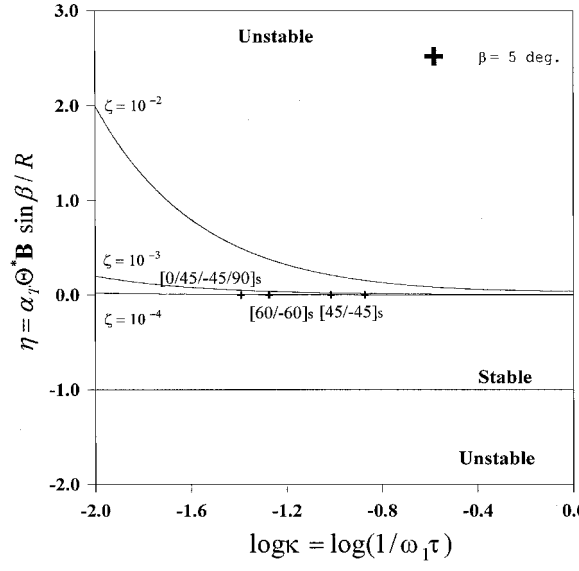

Fig. 14 Stability boundary with respect to the ply angles of the composite beam.

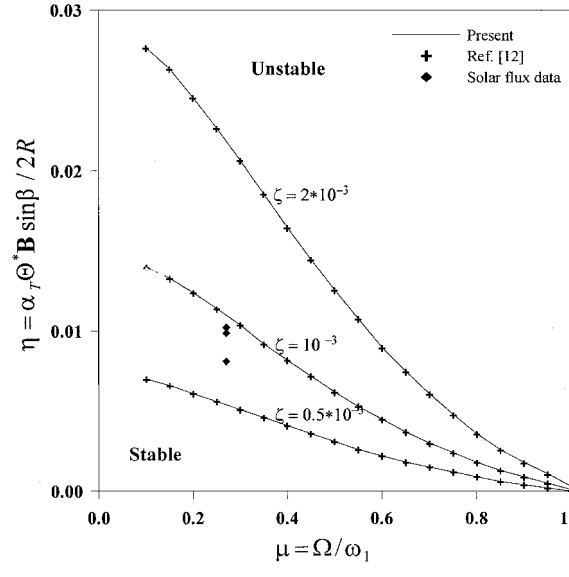

Fig. 15 Stability boundary for the spinning speed of the isotropic beam.

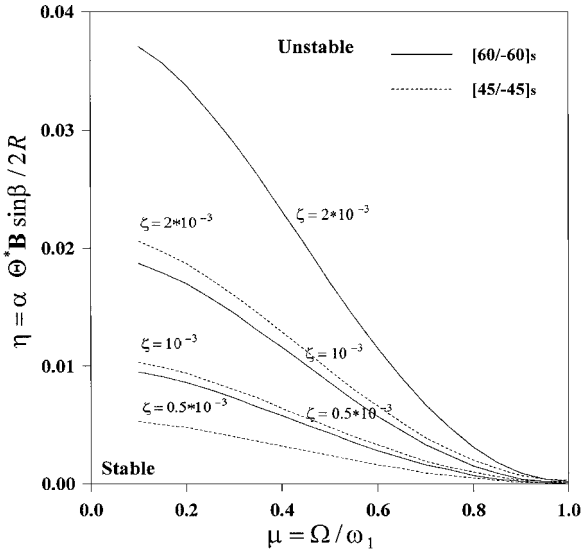

Fig. 16 Stability boundary for the spinning speed of the composite beam.

the stability boundaries of the spinning composite beam with respect to various stacking sequences of the materials. The solid line is the $[60/-60]_s$ sequence with $\kappa = 0.0532$, and the dotted line indicates the $[45/-45]_s$ sequence with $\kappa = 0.0964$. The stacking sequence of $[60/-60]_s$ has a wider stable region than the $[45/-45]_s$ sequence does. As a result, the stability boundary of the spinning composite beam depends on the stacking sequence of the materials and the spinning speed.

Conclusions

Coupled thermal–structural analysis of the spinning thin-walled composite beam appendage with the sudden solar heat flux is performed. Additionally, the dynamic response and the stability characteristics are investigated. Based on the numerical data, the results are summarized as follows:

Coupled thermal–structural analysis of the beam appendages must be performed to analyze unstable motions that may be induced by the sudden thermal loading.

The effects of the solar incident angle and stacking sequence of the composite materials are studied in the dynamic analysis. The deflection of the beam decreases, as the solar heat flux absorbed by the beam decreases. In addition, the appropriate stacking sequence of the composite materials may reduce the quasi-static and dynamic deflections of the beam.

The stable region of the beam depends on the stacking sequence of the composite materials, the damping coefficient, and the spinning speed. Thus, the stable region can be increased by controlling these factors. Furthermore, the spinning speed plays an important role in the stability criterion of the spinning beam under the solar heat flux. If the spinning speed equals the bending frequency of the beam, the beam structure is unconditionally unstable.

Acknowledgment

This work was supported by the Brain Korea 21 project.

References

[1]Tsuchiya, K., "Thermally Induced Vibrations of a Flexible Appendage Attached to a Spacecraft," *AIAA Journal*, Vol. 15, No. 4, 1977, pp. 505–510.

[2]Johnston, J. D., and Thornton, E. A., "Thermally Induced Attitude Dynamics of a Spacecraft with a Flexible Appendage," *Journal of Guidance, Control, and Dynamics*, Vol. 21, No. 4, 1998, pp. 581–587.

[3]Chung, P. W., and Thornton, E. A., "Torsional Buckling and Vibrations of a Flexible Rolled-Up Solar Array," *Proceedings of 37th AIAA/ASME/ASCE/AHS/ASC Structures, Structural Dynamics, and Materials Conference*, AIAA, Washington, DC, 1995, pp. 1654–1664; also AIAA Paper 95-1355, 1995.

[4]Boley, B. A., "Thermally Induced Vibrations of Beams," *Journal of the Aeronautical Sciences*, Vol. 3, No. 2, 1956, pp. 179–181.

[5]Boley, B. A., "Approximate Analyses of Thermally Induced Vibrations of Beams and Plates," *Journal of Applied Mechanics*, Vol. 39, No. 2, 1972, pp. 212–216.

[6]Tamma, K. K., Spyrakos, C. C., and Lambi, M. A., "Thermal/Structural Dynamic Analysis via a Transform-Method-Based Finite-Element Approach," *Journal of Spacecraft and Rockets*, Vol. 24, No. 3, 1987, pp. 219–226.

[7]Manolis, G. D., and Beskos, D. E., "Thermally Induced Vibrations of Beam Structures," *Computer Methods in Applied Mechanics and Engineering*, Vol. 21, No. 3, 1980, pp. 337–355.

[8]Lutz, J. D., Allen, D. H., and Haisler, W. E., "Finite-Element Model for the Thermoelastic Analysis of Large Composite Space Structures," *Journal of Spacecraft and Rockets*, Vol. 24, No. 5, 1987, pp. 430–436.

[9]Thornton, E. A., and Kim, Y. A., "Thermally Induced Bending Vibrations of a Flexible Rolled-Up Solar Array," *Journal of Spacecraft and Rockets*, Vol. 30, No. 4, 1993, pp. 438–448.

[10]Thornton, E. A., Chini, G. P., and Gulick, D. W., "Thermally Induced Vibrations of a Self-Shadowed Split-Blanket Solar Array," *Journal of Spacecraft and Rockets*, Vol. 32, No. 2, 1995, pp. 302–311.

[11]Leung, A. Y. T., and Fung, T. C., "Spinning Finite Elements," *Journal of Sound and Vibration*, Vol. 125, No. 3, 1988, pp. 523–537.

[12]Gulick, D. W., and Thornton, E. A., "Thermally Induced Vibrations of a Spinning Spacecraft Boom," *Acta Astronautica*, Vol. 36, No. 3, 1995, pp. 163–176.

[13]Farmer, J. T., Wahls, D. M., and Wright, R. L., "Thermal Distortion Analysis of an Antenna-Support Truss in Geosynchronous Orbit," *Journal of Spacecraft and Rockets*, Vol. 29, No. 3, 1992, pp. 386–393.

[14]Givoli, D., and Rand, O., "Thermoelastic Analysis of Space Structures in Periodic Motion," *Journal of Spacecraft and Rockets*, Vol. 28, No. 4, 1991, pp. 457–464.

[15]Thornton, E. A., and Paul, D. B., "Thermal–Structural Analysis of Large Space Structures: An Assessment of Recent Advances," *Journal of Spacecraft and Rockets*, Vol. 22, No. 4, 1985, pp. 385–393.

[16]Givoli, D., and Rand, O., "Minimization of Thermoelastic Deformation in Space Structures Undergoing Periodic Motion," *Journal of Spacecraft and Rockets*, Vol. 32, No. 4, 1995, pp. 662–669.

[17]Song, O. L., and Librescu, L., "Free Vibration of Anisotropic Composite Thin-Walled Beams of Closed Cross-Section Contour," *Journal of Sound and Vibrations*, Vol. 167, No. 1, 1993, pp. 129–147.

[18]Bathe, K. J., *Finite Element Procedures*, Prentice Hall, Upper Saddle River, NJ, 1996, pp. 493, 494, 780–782.

A. Berman
Associate Editor